



TIME-DOMAIN REPRESENTATION OF A FLAME TRANSFER FUNCTION WITH GENERALISED $n\tau$ -LAW FEATURING A TIME-LAG DISTRIBUTION

Sreenath Malamal Gopinathan, Alessandra Bigongiari and Maria A. Heckl

School of Computing and Mathematics, Keele University, Staffordshire, ST5 5BG, United Kingdom

email: s.malamal.gopinathan@keele.ac.uk

The aim of present work is to develop a method to determine the heat release law in the time-domain, from the measured/simulated Flame Transfer Function (FTF) in the frequency-domain. The present work is an extension of the famous $n\tau$ - law for heat release rate fluctuations. The heat release law is assumed to have a time-lag (τ) distribution, where the coupling coefficients (n) themselves depend on the time-lag distribution in a piecewise constant manner. The flame transfer function of the heat release law in the frequency-domain is obtained from Fourier transformation of its time-domain representation. The coupling coefficients (n) are evaluated using Mean Square Error (MSE) minimisation method, by comparing the modelled Flame Transfer Function with experimental/simulated data. In our study, we use the Flame Transfer Function for conical and V-flames, developed by Schuller et al. (Combustion and Flame, 134(1-2), 21-34, 2003).

1. Introduction

In order to reduce pollution of the environment by combustion exhaust gases, power generation systems operate with lean premixed flames. However, such systems are susceptible to thermoacoustic instabilities, which are high-amplitude oscillations caused by the feedback between oscillations in pressure and in heat release rate, and which can cause major hardware damage.

The relationship between the heat release rate and the acoustic field is a crucial element in modelling thermoacoustic instabilities. This relationship is commonly described by the flame transfer function (FTF), which is a frequency-domain quantity. We use the following notation: $Q'(t)$ is the fluctuation of the heat release rate in the time-domain, $\hat{Q}(\omega)$ is its frequency-domain equivalent (Fourier transform), and \bar{Q} is the mean rate of heat release; the same notation is used for the acoustic velocity, v . The FTF is the ratio of (non-dimensional) heat release rate, $\hat{Q}(\omega)/\bar{Q}$, of the flame, to (non-dimensional) velocity fluctuations, $\hat{v}(\omega)/\bar{v}$, at a reference position upstream of the flame.

A simple time-lag law for the heat release rate, with a time delayed term and an instantaneous term in acoustic velocity was developed for a matrix burner flame, by Heckl [1, 2, 3]. Even though the model captured the relevant features of the transfer function, the low pass behaviour of the FTF was not predicted. Nevertheless, their model predicted the stability maps of the burner in line with the measured stability maps. Blumenthal et al. [4] and Subramanian et al. [5] have examined the linear response of premixed flames using discrete time-lag and impulse response (IR) functions. Computational fluid dynamics (CFD) and system identification were combined to characterise the dynamic response of systems in [6]. The systems were treated as black boxes and an IR functions approach was employed to study a swirl burner.

In this paper, we propose a new method to convert a given FTF into a heat release law in the time-domain. The underlying idea is based on a simple physical observation: flow perturbations

travelling from a reference position to the flame do not all cover the same distance with the same velocity, and therefore they arrive at the flame with a *distribution* of time-lags. Our method will give the heat release law in terms of a small number of parameters, and this is well-suited for analytical modelling of thermoacoustic instabilities.

We explain the method in section 2 and apply it to some basic test cases in section 3. This application will not only validate our method, but provide better physical insight into the behaviour of laminar flames (conical flames, V-flames) studied by Schuller et al. [7].

2. Heat release law with distributed time-lag

The generalised heat release law with a distributed time-lag is assumed to be of the form

$$\frac{Q'(t)}{\bar{Q}} = \frac{1}{\tau_{max}} \int_0^{\tau_{max}} n(\tau) \frac{v'(t-\tau)}{\bar{v}} d\tau, \quad (1)$$

where τ is the time-lag and n is the coupling coefficient, which is a real number. τ_{max} is a time scale associated with the physical process being investigated. We divide the integration range $[0, \tau_{max}]$ into k intervals of length $\Delta\tau$ and assume that the coupling constant n is uniform in each interval, for example: $n(\tau) = n_1$ for $\tau \in [0, \Delta\tau]$, $n(\tau) = n_2$ for $\tau \in [\Delta\tau, 2\Delta\tau]$, etc. In other words, we treat $n(\tau)$ as a piecewise constant function. We can then split integral in Eq. (1) into a sum of k integrals and write

$$\frac{Q'(t)}{\bar{Q}} = \frac{1}{\tau_{max}} \left[n_1 \int_0^{\Delta\tau} \frac{v'(t-\tau)}{\bar{v}} d\tau + n_2 \int_{\Delta\tau}^{2\Delta\tau} \frac{v'(t-\tau)}{\bar{v}} d\tau + \dots + n_k \int_{(k-1)\Delta\tau}^{k\Delta\tau} \frac{v'(t-\tau)}{\bar{v}} d\tau \right]. \quad (2)$$

The flame transfer function (FTF) in the frequency domain, defined as $\mathcal{T}(\omega) = \frac{\hat{Q}(\omega)}{\bar{Q}} / \frac{\hat{v}(\omega)}{\bar{v}}$, is obtained by taking the Fourier transform of Eq. (2).

$$\frac{\hat{Q}(\omega)}{\bar{Q}} = \left\{ \frac{1}{\tau_{max}} e^{-i\omega \frac{\Delta\tau}{2}} \frac{2}{\omega} \sin(\omega \frac{\Delta\tau}{2}) [n_1 e^{i\omega \Delta\tau} + n_2 e^{2i\omega \Delta\tau} + \dots + n_k e^{ki\omega \Delta\tau}] \right\} \frac{\hat{v}(\omega)}{\bar{v}}. \quad (3)$$

$$\therefore \mathcal{T}_k(\omega) = \frac{1}{\tau_{max}} e^{-i\omega \frac{\Delta\tau}{2}} \frac{2}{\omega} \sin(\omega \frac{\Delta\tau}{2}) [n_1 e^{i\omega \Delta\tau} + n_2 e^{2i\omega \Delta\tau} + \dots + n_k e^{ki\omega \Delta\tau}]. \quad (4)$$

Typically, $\mathcal{T}(\omega)$ is obtained from experiments or simulations. In order to describe the heat release law in the time-domain, we require the coupling coefficients, n_1, n_2, \dots, n_k . They are evaluated by minimising the mean square error (MSE) between the modelled $\mathcal{T}_k(\omega)$ (Eq. (4)) and the measured $\mathcal{T}(\omega)$ from experiments or simulations. The MSE in the frequency range $[0, \omega_{max}]$ is given by $\epsilon_k = \int_0^{\omega_{max}} [\mathcal{T}(\omega) - \mathcal{T}_k(\omega)]^2 d\omega$. Minimising the MSE gives a matrix equation in n_1, n_2, \dots, n_k . The solution of this matrix equation give the values of n_1, n_2, \dots, n_k . The value of τ_{max} and the number of equal divisions k (or the value of $\Delta\tau$) is selected according to inherent physical features of the problem studied.

3. Application to specific flames

The heat release law with distributed time-lag described in section 2 can be applied to any flame with a known FTF in the frequency domain. In the present work, the distributed time-lag model for heat release has been applied to two specific flames : Conical and V-flames (Fig. 1). Even though these flames are simple and basic, they help us in demonstrating the usability of our method in explaining the physical processes involved. This allows for the extension of the present method to other practical

flames we encounter. The two flames are subjected to two different perturbations, namely uniform velocity perturbation and axial convective velocity perturbation. Analytical expressions as well as numerical simulations for the FTFs of conical and V-flames under different velocity perturbations are given in Schuller et al.[7]. We make use of these analytical expressions to estimate the coupling coefficients of our modelled FTF. The flame is anchored at the burner rim for a conical flame and at the central rod for a V-flame. This corresponds to a zero displacement boundary condition at the flame base [7].



Figure 1: Schematic of different flame shapes

3.1 Conical flames

Conical flames are formed when the flame anchors on the rim of a circular burner duct (Fig. 1(a)). The flame front is the location where the laminar flame velocity (S_L) balances with the flame-normal component of the velocity of fuel-air mixture through the duct (\bar{v}). For any particular fuel-air mixture, S_L is taken as a constant. Therefore, given \bar{v} , we can find the flame angle $\alpha = \sin^{-1}(S_L/\bar{v})$.

3.1.1 Uniform velocity perturbation

The analytical expression for the FTF of a uniformly perturbed flame is [7]

$$\mathcal{T}(\omega)_{UCO} = \frac{2}{\omega_*^2} [1 - \exp(i\omega_*) + i\omega_*], \quad (5)$$

where,

$$\omega_* = (\omega R)/(S_L \cos \alpha). \quad (6)$$

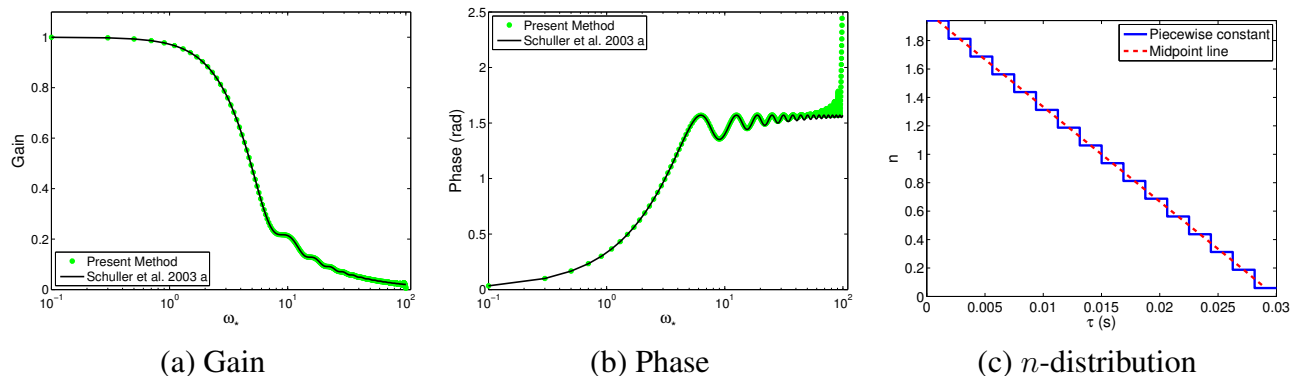


Figure 2: Variation of Gain and Phase of the FTF as a function of ω_* and the distribution of n for uniformly perturbed conical flame ($\alpha = 20^\circ$). The $--$ line in (c) connects the midpoints of all the piecewise constant n values.

The reduced frequency ω_* , is a dimensionless parameter, R is the radius of the burner duct (Fig. 1(a)) and ω is the frequency of the perturbation. The gain and phase of the FTF (analytical) are shown as solid black lines in Fig. 2 (a,b). The conditions assumed are : $S_L = 0.39 \text{ m/s}$, $\alpha = 20^\circ$,

$R = 11 \text{ mm}$, $n = \{n_1, n_2, \dots, n_{16}\}$, $\Delta\tau = \tau_{max}/16$. We then evaluated the coupling coefficients for the FTF in Eq. (5). The corresponding modelled FTF (green dots) as well as the resulting n distribution are shown in Fig. 2 (a,b) and Fig. 2 (c), respectively. We can define a perturbation time scale as $\tau_{pert} = (R/\sin \alpha)/(\bar{v} \cos \alpha) = R/(S_L \cos \alpha)$, which is the time taken for a perturbation to travel from the root to the tip of the flame, along the flame front with a velocity $\bar{v} \cos \alpha$. In our study, we have taken $\tau_{max} = \tau_{pert} = R/(S_L \cos \alpha)$. This is taken as the characteristic time scale of the flame and is applicable to all the flames considered in the present work.

3.1.2 Axial convective velocity perturbation

For axially convected perturbation, we use [7]

$$\mathcal{T}(\omega)_{CCO} = \frac{2}{\omega_*^2} \frac{1}{1 - \cos^2 \alpha} \left[1 - \exp(i\omega_*) + \frac{\exp(i\omega_* \cos^2 \alpha) - 1}{\cos^2 \alpha} \right]. \quad (7)$$

Here, the FTF depends on both reduced frequency, ω_* and flame angle, α . Figure 3 (a,b) show the analytical (black line) and modelled FTF (green dots) for a small flame angle, $\alpha = 20^\circ$ and Fig. 3 (c) shows the corresponding n distribution. Figure 4 shows the same for a larger flame angle, $\alpha = 80^\circ$. From these two results it can be observed that the distribution of n is significantly different from what we observed in the uniformly perturbed case. The peak value of n occurs at larger τ value for small flame angle, and the peak shifts to smaller τ with increasing flame angles. The distribution of n tends to that of uniformly perturbed case for α close to 90° . This behaviour will be explained in detail in section 4.

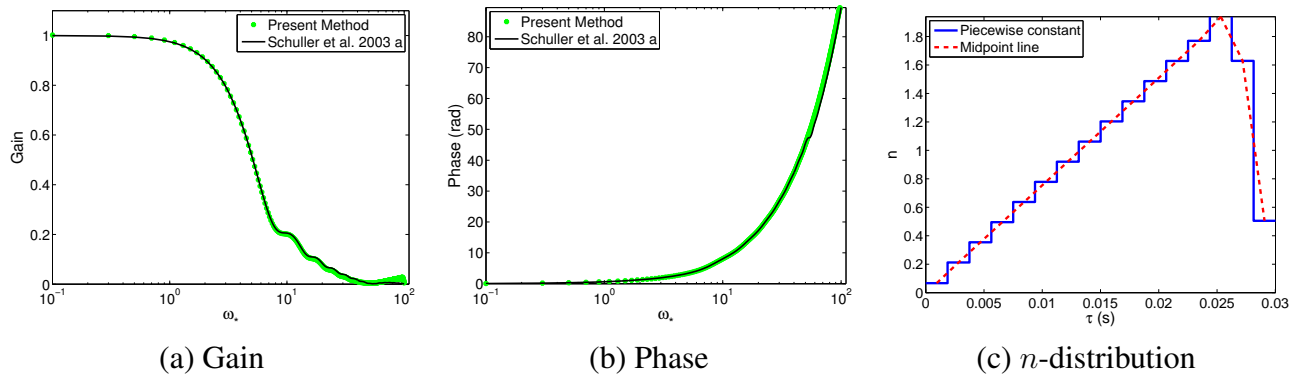


Figure 3: Variation of Gain and Phase of the FTF as a function of ω_* and the distribution of n for conical flame with axial convective perturbation and $\alpha = 20^\circ$. The $--$ line in (c) connects the midpoints of all the piecewise constant n values.

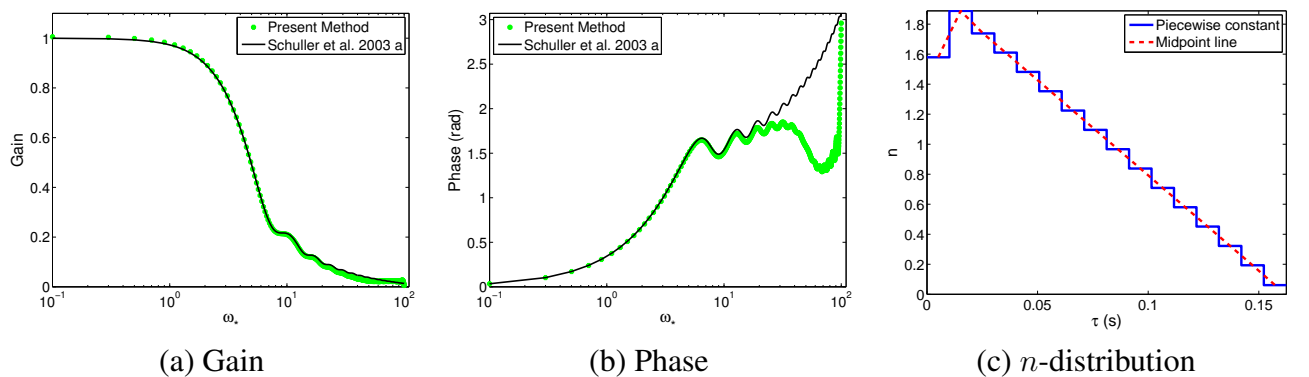


Figure 4: Variation of Gain and Phase of the FTF as a function of ω_* and the distribution of n for conical flame with axial convective perturbation and $\alpha = 80^\circ$. The $--$ line in (c) connects the midpoints of all the piecewise constant n values.

3.2 V-flames

V-flames are formed when the flame anchors on a rod concentric to a circular burner duct (Fig. 1(b)). We use the same notations for the flame angle α and other parameters as in conical flame, since the geometries are similar except of the locations of the burner axes or the lines of symmetry.

3.2.1 Uniform velocity perturbation

The analytical expression for the FTF of a uniformly perturbed V-flame is [7]

$$\mathcal{T}(\omega)_{UVR} = \frac{2}{\omega_*^2} \left[\frac{b-a}{b+a} (\exp(i\omega_*) - 1) + i\omega_* \left(\frac{a}{b+a} - \frac{b}{b+a} \exp(i\omega_*) \right) \right], \quad (8)$$

where a is the radius of the rod placed within the burner and b is the burner radius (Fig. 1(b)). The conditions assumed are : $S_L = 0.39 \text{ m/s}$, $\alpha = 20^\circ$, $a = 3 \text{ mm}$, $b = 11 \text{ mm}$, $R = b - a$, $n = \{n_1, n_2, \dots, n_{16}\}$, $\Delta\tau = \tau_{max}/16$. Figure 5 (a,b) shows the comparison between the analytical and modelled FTF for a uniformly perturbed V-flame. Figure 5(c) shows the n distribution for this case.

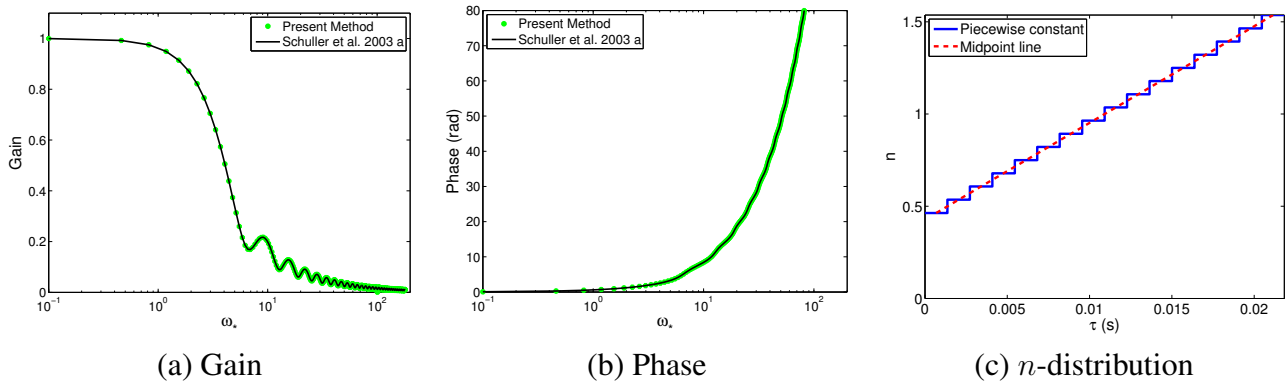


Figure 5: Variation of Gain and Phase of the FTF as a function of ω_* and the distribution of n for uniformly perturbed V-flame ($\alpha = 20^\circ$). The $--$ line in (c) connects the midpoints of all the piecewise constant n values.

3.2.2 Axial convective velocity perturbation

For axially convected perturbations in V-flames [7], the FTF is given by,

$$\begin{aligned} \mathcal{T}(\omega) = & \frac{2}{\omega_*^2} \frac{1}{1 - \cos^2 \alpha} \frac{b-a}{b+a} \left[\exp(i\omega_*) - 1 - \frac{\exp(i\omega_* \cos^2 \alpha) - 1}{\cos^2 \alpha} \right] \\ & + \frac{2i}{\omega_*} \frac{1}{1 - \cos^2 \alpha} \frac{b}{b+a} \left[\exp(i\omega_* \cos^2 \alpha) - \exp(i\omega_*) \right]. \end{aligned} \quad (9)$$

Like axially convected conical flames, the FTF of V-flames depends on both reduced frequency, ω_* and flame angle, α . In addition to this, the FTF also depends on the diameter of the rod a and the diameter of the burner b . Figures 6 and 7 show the comparison between analytical and modelled FTF for V-flames with flame angles 20° and 80° respectively. For axial convective perturbation, we observe that the value of n is negative till a certain value of τ and then becomes positive. As α increases, the time till which n has negative values decreases and the behaviour tends to that of uniformly perturbed case as α approaches 90° .

4. Physical insight to the behaviour of the flame

From the previous section, it is evident that the distributed time-lag model gives accurate prediction of the FTF in the frequency domain for all flame types and perturbations considered. The n

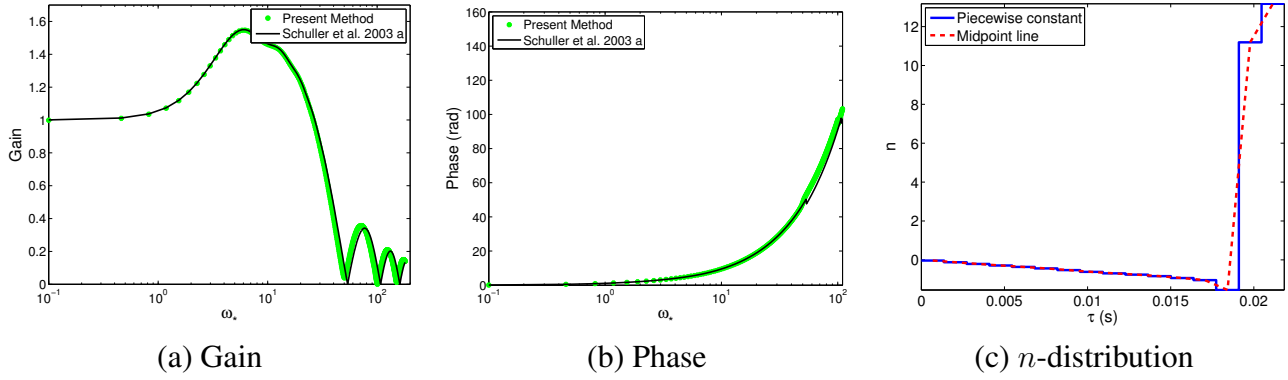


Figure 6: Variation of Gain and Phase of the FTF as a function of ω_* and the distribution of n for V-flame with axial convective perturbation and $\alpha = 20^\circ$. The $--$ line in (c) connects the midpoints of all the piecewise constant n values.

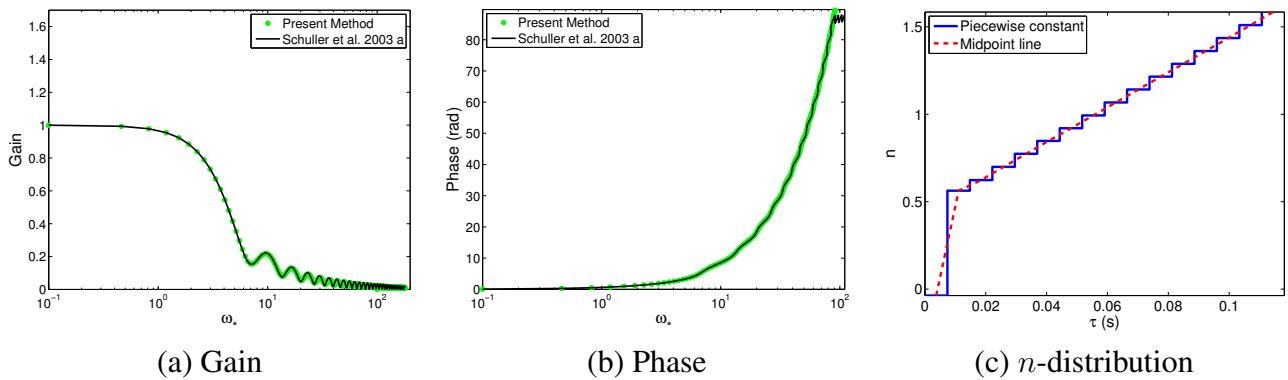


Figure 7: Variation of Gain and Phase of the FTF as a function of ω_* and the distribution of n for V-flame with axial convective perturbation and $\alpha = 80^\circ$. The $--$ line in (c) connects the midpoints of all the piecewise constant n values.

distributions we obtained, enable us to construct the heat release law in the time-domain. The variation of $n(\tau)$ with τ gives physical insight into the behaviour of conical and V-flames subjected to perturbations. The variation of $n(\tau)$ is different in each case and so is the behaviour. The fluctuations in heat release rate is proportional to the fluctuations in flame surface area caused by the velocity perturbations [7]. Hence, the relation between the n distribution and the flame dynamics can be explained in terms of the flame surface area.

4.1 Conical flames

Figure 8 shows the perturbed flame shapes when subjected to uniform and axial convective perturbations and also the corresponding n distribution. Under uniform perturbation, the flame elongates and contracts with the perturbation. In such a case, the maximum change in flame surface area happens at regions near the flame base. When viewed in the time domain, this maximum area change occurs at the initial time when a perturbation leaves the burner rim. This explains the peak value of n at the lowest τ for uniformly perturbed flames (Fig. 8(b)). However, in the case of an axial convective perturbation, we have a perturbation convecting with a velocity $\bar{v}/\cos\alpha$ along the flame front of length $R/\sin\alpha$. This gives a convective time of $\tau_{conv} = R\cos\alpha/S_L$. Looking at the flame shape of the axial convective perturbed flame, we can observe that the flame surface area experiences a maximum when the perturbation reaches the tip of the flame. This occurs at the time, τ_{conv} , which is clearly the time instant at which the $n(\tau)$ distribution for the axial convective case has a peak value (Fig. 8). The parameters used are : $S_L = 0.39$ m/s, $\alpha = 20^\circ$, $R = 11$ mm, $n = \{n_1, n_2, \dots, n_{16}\}$,

$\Delta\tau = \tau_{max}/16$, $\tau_{max} = 0.03s$, $\tau_{conv} = 0.0265s$. As α increases, τ_{conv} decreases. For flame angles close to 90° , the convective effects are negligible ($\tau_{conv} \rightarrow 0$) as the flame front is almost perpendicular to the velocity perturbation and thus the flame tends to behave as a uniformly perturbed flame. The shape of the $n(\tau)$ distribution is similar to the shape of the IR functions obtained by Blumenthal et al [4].

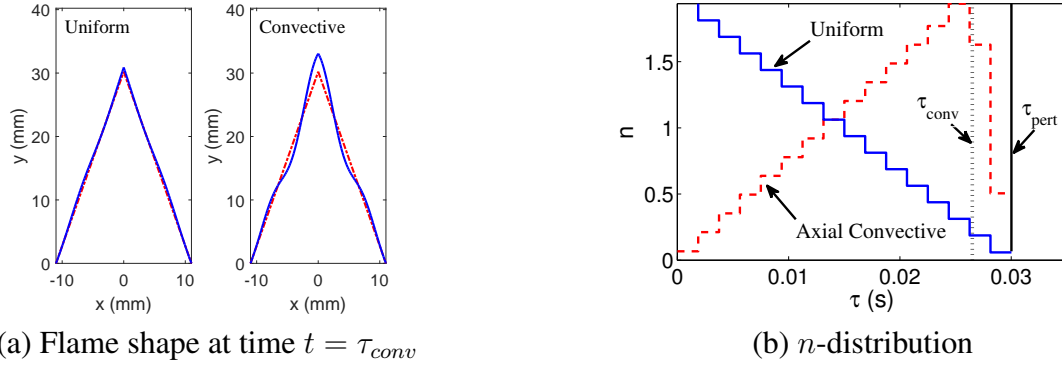


Figure 8: Flame shapes and variation of n for uniform perturbation and axial convective perturbation for a conical flame. The red curve in (a) shows the steady state flame.

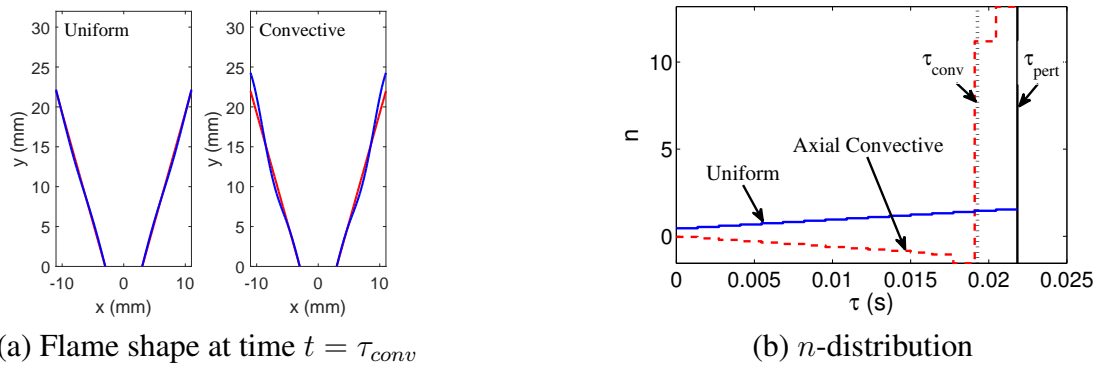


Figure 9: Flame shapes and variation of n for uniform perturbation and axial convective perturbation for a V-flame. The red curve in (a) shows the steady state flame.

4.2 V-flames

Figure 9 shows the perturbed flame shapes and n distribution for a V-flame. The behaviour of V-flames can be explained using the same approach as in conical flames. For uniformly perturbed V-flames, the flame elongates and contracts with the perturbation. Unlike the conical flames, the maximum change in flame surface area happens at the flame tip. In the time domain, this maximum area change occurs at the time instant close to τ_{pert} (Fig. 9(b)). This explains the peak value of n close to τ_{pert} for a uniformly perturbed V-flames. For an axial convective perturbation, the perturbation is convected along the flame front with at velocity $\bar{v}/\cos\alpha$. This is similar to the conical flame and in this case $R = b - a$ (Fig. 1(b)). The convective time for V-flames is $\tau_{conv} = R \cos\alpha / S_L$. From the flame shape of axial convective perturbed flame, the maximum change in flame surface area happens when the perturbation reaches the tip of the flame, which is at τ_{conv} . But, the $n(\tau)$ distribution for the V-flame has negative values in the initial time range, till τ_{conv} . The sign of n then changes to a positive value and remains positive for $\tau > \tau_{conv}$. As the convective perturbation propagates along the flame front, from the flame anchor point, it causes a decrease in area which in turn decreases the heat release rate. Hence, the negative sign for n values till τ_{conv} . The parameters used are : $S_L = 0.39m/s$, $\alpha = 20^\circ$, $a = 3mm$, $b = 11mm$, $R = b - a$, $n = \{n_1, n_2 \dots n_{16}\}$, $\Delta\tau = \tau_{max}/16$, $\tau_{max} = 0.0218s$,

$\tau_{conv} = 0.0193s$. When α increases τ_{conv} decreases and the time at which n changes to positive values decreases. As α approaches 90° , the convective effects are negligible and the flame tends to behave as a uniformly perturbed flame. This behaviour is similar to what we observe for conical flames. In this case too, the shape of the $n(\tau)$ distribution is similar to the shape of the IR functions obtained by Blumenthal et al. [4].

5. Conclusions

A time domain representation of a generalised heat release law with time-lag distribution was developed and its corresponding FTF in the frequency domain was obtained. This model was applied to conical and V-flames subjected to uniform and axial convective velocity perturbations. The model parameters ($n = \{n_1, n_2, \dots, n_k\}$) were determined, by minimising the mean square error (MSE) between the analytical FTF and the modelled FTF. The distributed time lag model in the time domain gives a good insight into the physical behaviour of the fundamental flames experiencing velocity perturbations. Our results are similar to the IR functions given in [4], for conical and V-flames. The values of τ_{max} and $\Delta\tau$ were chosen based on the process and its physical features. The method can be extended to more practical cases like the matrix burner flames, swirl flames, and also to heat exchanger transfer functions. Work is in progress to determine the best values for τ_{max} and $\Delta\tau$ from measured or simulated FTF and provide a more generic formulation.

Acknowledgements

The presented work is part of the Marie Curie Initial Training Network Thermoacoustic and Aeroacoustic Nonlinearities in Green combustors with Orifice structures (TANGO). We gratefully acknowledge the financial support from the European Commission under call FP7-PEOPLE-ITN-2012.

REFERENCES

1. Heckl, M. A. Analytical model of nonlinear thermo-acoustic effects in a matrix burner, *Journal of Sound and Vibration*, **332** (17), 4021–4036, (2013).
2. Heckl, M. A new perspective on the flame describing function of a matrix flame, *International Journal of Spray and Combustion Dynamics*, **7** (2), 91–112, (2015).
3. Heckl, M. A. Analytical model of nonlinear thermoacoustic effects in a matrix burner, *n³l - International Summer School and Workshop on Non-Normal and Nonlinear Effects in Aero- and Thermoacoustics*, Munich, June 18-21, (2013).
4. Blumenthal, R. S., Subramanian, P., Sujith, R. and Polifke, W. Novel perspectives on the dynamics of premixed flames, *Combustion and Flame*, **160** (7), 1215 – 1224, (2013).
5. Subramanian, P., Blumenthal, R. S., Polifke, W. and Sujith, R. I. Distributed time lag response functions for the modeling of combustion dynamics, *Combustion Theory and Modelling*, **19** (2), 223–237, (2015).
6. Polifke, W. Black-box system identification for reduced order model construction, *Annals of Nuclear Energy*, **67**, 109–128, (2014).
7. Schuller, T., Durox, D. and Candel, S. A unified model for the prediction of laminar flame transfer functions: comparisons between conical and v-flame dynamics, *Combustion and Flame*, **134** (1–2), 21 – 34, (2003).